Linear response of the human erythrocyte to mechanical stress

Mark A. Peterson
Mount Holyoke College, South Hadley, Massachusetts 01075
(Received 17 October 1991)

The human erythrocyte readily changes its shape in response to mechanical stress. Geometrical methods are used to analyze this effect in three experiments: thermal shape fluctuation (flicker), electrodeformation, and tank treading, which is the circulation of the membrane around the interior fluid in a shear flow. Comparison with existing data indicates that both flicker and tank treading represent the motion of a fluid membrane. At the same time it is a solid membrane (i.e., possessing a shear modulus) that resists large-scale shape change. This combination of fluid and solid membrane properties is in some ways paradoxical.

PACS number(s): 87.22.Bt, 87.45.Bp

I. INTRODUCTION

The mechanical properties of the red-blood-cell (erythrocyte) membrane have been investigated intensively for many years [1,2]. On the basis of the micropipette-aspiration method of Evans, Hochmuth, and others, the membrane has been assigned a shear modulus $\mu=6-9\times10^{-6}$ N/m, a bending modulus $k_c=2\times10^{-19}$ J, and a two-dimensional viscosity $\eta_M=0.6-1.2\times10^{-6}$ N s/m. It is regarded variously as a viscoelastic solid [1], or a two-dimensional gel [3].

More recently there has been considerable theoretical interest in the dynamics of membranes, including also artificial lipid vesicles and tethered two-dimensional (2D) polymers [4,5]. A key role in these investigations is played by the entropy of shape fluctuations [6], which can make an appreciable contribution to the membrane free energy. These entropic effects have been observed in experiments on erythrocytes [7]. The erythrocyte membrane and modifications of it are natural model systems to test these theories.

As a material the membrane is a composite of lipid, protein, and other macromolecules. The original fluid mosaic model of Singer and Nicolson [8] emphasized the fluidity of the membrane, identifying the fluid lipid bilayer as the matrix in which the dissolved (integral) membrane proteins move. The experimental picture that has emerged, however, gives considerable importance to proteins which are not integral, notably the protein spectrin that forms a network on the interior surface of the erythrocyte membrane called the cytoskeleton [9]. The interaction of the lipid component and the cytoskeleton is still not well understood.

Other techniques besides micropipette aspiration have been used to investigate the mechanical properties of the erythrocyte membrane, for example quantitative studies of erythrocyte flicker [10,11], deformation in a high-frequency electric field [12], and deformation in a shear flow [13,14]. These experiments are, in principle, simpler than micropipette aspiration in that the local strains can be kept small so that linear theory ought to apply. (A nonlinear phenomenological stress-strain relationship has always been used in interpreting the micropipette experiments). In these linear experiments there is also no suppression of modes, with a corresponding entropic contribution to the change in free energy, as may happen when the membrane adheres to the glass wall of a micropipette. Thus the interpretation of these experiments is, in principle, more straightforward. In practice, however, it has not been possible to make meaningful comparisons of these experiments with each other or with the micropipette experiments because of large theoretical uncertainties in the analysis. These uncertainties arise when the geometry of the membrane shape is not handled accurately.

The natural language to describe smooth surfaces is differential geometry. More than a language, differential geometry provides methods of computation, such as the Lie derivative, that are extremely efficient. These methods are not as well known as they might be because it is usually possible in physical models to consider only the simplest geometries—planes, spheres, cylinders, or at worst ellipsoids—for which general methods are unnecessary. The erythrocyte response to stress appears to be an exceptional problem in actually requiring differential geometry for an adequate treatment. Previous analyses have always been recognized as approximate, and it is not possible to assess the meaning of the various erythrocyte experiments as long as this uncertainty persists. This means one must apply the methods of differential geometry.

In this paper I deal with the geometric problems that arise in the analysis of several experiments essentially without approximation. In this way a large amount of data, which has been of only semiquantitative significance until now, assumes quantitative importance, and can be compared with the micropipette data. One sees something that does not show up in the micropipette experiments, namely clear evidence for a fluid component in the erythrocyte membrane. One also finds, in the linear experiments, a shear modulus for the solid component which is almost an order of magnitude smaller than is seen with the micropipette technique. The reason for this discrepancy is not clear, but the discrepancy is real.

I turn first to the geometrical methods, in Sec. II–IV and later VII. These sections mainly set up notation and make explicit the assumptions which go into the computations. They assume some familiarity with geometry. For the classical geometry of surfaces the book of Willmore [15] is a good reference. For the Lie derivative, Hodge star operator, and differential forms, the book of Schutz [16] is excellent. Flicker amplitudes are analyzed in Sec. V, electrodeformation in Sec. VI, tank treading, which is the circulation of the membrane around the interior fluid in a shear flow in Sec. VIII, and hydrodynamic flicker decay modes in Sec. IX. Section X is a summary and conclusion. Additional details of the computational methods are in the appendixes.

II. GEOMETRY

The erythrocyte shape is a surface of revolution M with reflection symmetry in the equatorial plane. Thus it can be generated by a curve

$$C(s)=[x(s),y(s)] \tag{1}$$

in the first quadrant of the x-y plane, using the x axis as a rotation axis, and the y-z plane as an equatorial plane, as shown in Fig. 1. The pair (s,ψ) furnishes coordinates on M, where s is the arclength along C and ψ is the azimuthal angle. s is scaled so that C has length $\pi/2$. For any given cell this scaling fixes a unit of length which I call R. R is approximately, but not exactly, the radius the cell would have if it were swollen to a sphere with the same area. (s,ψ) on M are analogous to spherical polar coordinates on the sphere, and the spherical harmonics $Y_{lm}(s,\psi)$ are a convenient, although not orthogonal, basis in $L^2(M)$. This basis restricts to give bases in the subspaces of definite symmetry under reflection, inversion, and rotation about the symmetry axis.

Distance from M along the local outer normal defines a third coordinate n, so that (n,s,ψ) is a coordinate system in a tubular neighborhood of M. Associated to these coordinates there are bases in the tangent and cotangent bundles to $\mathbb{R}^3$, so that the Euclidean metric tensor G has the form

$$G=\mathrm{diag}[1,(1+c_1 n)^2,y^2(1+c_2 n)^2] . \tag{2}$$

Restricting to M, the first fundamental form g has the form

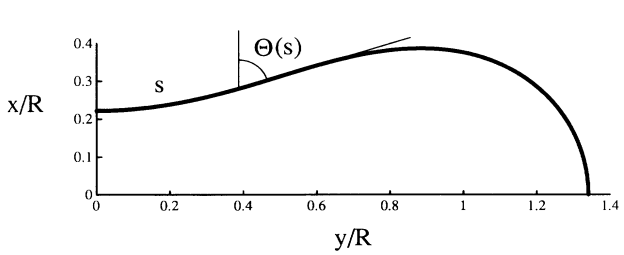

FIG. 1. Generating curve C for model cell shape, found by minimizing curvature energy. The cell shape corresponds to a RBC at 290 mOs with area 135 μm^2 and cell volume 96 μm^3, cell I in the computation.

$$g=\mathrm{diag}(1,y^2) \tag{3}$$

and the second fundamental form L of the surface has the form

$$L=\mathrm{diag}(c_1,c_2 y^2) . \tag{4}$$

Here

$$c_1=\frac{d\Theta}{ds} \tag{5}$$

and

$$c_2=-\frac{\cos\Theta}{y} \tag{6}$$

are the two principal curvatures. We recall the definitions of mean curvature H,

$$H=\mathrm{Tr}(L)/2=(c_1+c_2)/2 , \tag{7}$$

and Gauss curvature K,

$$K=\det(L)/\det(g)=c_1 c_2 . \tag{8}$$

Other useful geometric information, including explicit formulas for covariant differentiation on M, the Hodge star operator ($*$), the two-dimensional shear strain tensor S of a vector field X, and transformation to the Cartesian basis, are given in Appendix A.

III. VECTOR FIELDS ON M AND CONSTRAINTS

We can specify a motion of the membrane M, in first order, by specifying a vector field X on M, or equivalently a covector field (differential 1-form) $\tilde{X}$. The latter can always be written as

$$\tilde{X}=N dn+d\alpha+*d\beta , \tag{9}$$

where N, α, and β are functions of (s,ψ). The projection of these functions onto spaces of definite rotation and inversion symmetry will be written as $N_m^{\pm}$, $\alpha_m^{\pm}$, and $\beta_m^{\pm}$. Then there are explicit expansions

$$N_m^{\pm}(s,\psi)=\sum_l N_{lm}^{\pm} Y_{lm}(s,\psi) , \tag{10}$$

where the numbers N_{lm}^{+} are nonzero only if l is even, and the numbers N_{lm}^{-} are nonzero only if l is odd, etc.

These numbers cannot be chosen arbitrarily, however, because of constraints. In the experiments which I consider the stresses on the membrane are very small. As a consequence, the volume V and area A of the cell do not change appreciably, giving two integral constraints. It is an attractive hypothesis that also $\langle H\rangle$, the average of H over M, does not change, reflecting the incompressibility of each monolayer in the lipid bilayer membrane separately [17]. This possibility, which is a third integral constraint, will be called the "bilayer coupling hypothesis" (BCH). These integral constraints affect only $N_0^{+}(s,\psi)$, and require

$$\int_M N_0^{+} dA=0 \quad (V=\mathrm{const}) , \tag{11}$$

$$\int_M N_0^{+} H dA=0 \quad (A=\mathrm{const}) , \tag{12}$$

and, if $\langle H \rangle$ is constant,

$$\int_M N_0^+ K dA = 0 \quad \text{(BCH)} . \tag{13}$$

In addition to the integral constraints, there is a local constraint, local incompressibility of M, which requires

$$\mathrm{Tr}(S) = 0 , \tag{14}$$

where S is the two-dimensional strain of X. Using the representation Eq. (9) and the formulas of Appendix A this is

$$\Delta\alpha = 2NH , \tag{15}$$

where Δ is the Laplace-Beltrami operator of M. Because of Eq. (15) each $\alpha_m^\pm$ is a linear functional of the corresponding $N_m^\pm$. An explicit formula is given in Appendix B.

Let X and Y be vector fields on M. A useful inner product is

$$(X, Y) = \int_M \bar{X} \cdot Y dA . \tag{16}$$

With respect to this inner product one can construct orthonormal bases of vector fields which obey all constraints, as well as orthonormal bases on the orthogonal complement of this space. Explicit formulas are in Appendix B.

IV. ENERGIES

Much work on the elastic energy of the erythrocyte membrane indicates that both bending energy and shear energy are important in deformations at fixed area [1]. There is remarkable agreement between the observed equilibrium shapes of the erythrocyte and the stationary points of the bending energy

$$E_B = \frac{k_c}{2} \int_M (2H)^2 dA , \tag{17}$$

where k_c is the bending modulus [18,19,17]. The commonly seen stomatocyte shape, which has large principal curvatures but small mean curvature, and which does occur as a stationary shape of E_B [17], is particularly suggestive of the importance of the mean curvature. Apparently the shear energy can relax over time, and does not contribute to determining the equilibrium shape. Over short times, however, one expects from standard arguments of elasticity theory that a deformation will cost shear energy of the form

$$E_S = \mu \int_M S_{ij} S^{ij} dA , \tag{18}$$

where μ is the two-dimensional shear modulus.

In minimizing the total energy

$$E_{\text{tot}} = E_B + E_S \tag{19}$$

subject to constraints, one may introduce Lagrangian multiplier terms

$$-2c_0 k_c A \langle H \rangle + \sigma A - (\Delta p) V \tag{20}$$

but these are mathematical artifacts, not real energies. An exception is the first term, in case $\langle H \rangle$ really does change (i.e., in case the BCH does not hold). In that case one should regard that term as an energy, and c_0 as a kind of elastic modulus [20]. Of course if A and V were not constant, the other terms would represent energies too.

It should be pointed out that there are stationary shapes of E_B which are not observed for erythrocytes, but which are seen in artificial lipid vesicles [21]. Perhaps the cytoskeleton inhibits certain shape transitions (although interestingly not the stomatocyte transition).

Two model cells used in the computations for this paper are described in Appendix C.

To describe linear response of these cells one should expand the total energy to second order in a deformation

$$X = \sum_i a_i X^{(i)} \tag{21}$$

about the minimum, subject to the constraints. The first-order term vanishes, by stationarity, and the second-order term is a quadratic form in deformation coordinates, Hermitian with respect to the inner product Eq. (16). It is enough to do this within each symmetry class:

$$E_{\text{tot}}(X_m^\pm) = E_{\text{tot}}(0) + \tfrac{1}{2} \sum_{i,j} \bar{a}_i E_m^{\pm ij} a_j + \cdots . \tag{22}$$

The eigenvectors $a^{(k)}$ of this quadratic form satisfy

$$\sum_j E_m^{\pm ij} a_j^{(k)} = \lambda_k^\pm a_i^{(k)} \tag{23}$$

and determine the normal modes

$$U_m^{\pm(k)}(s, \psi) = \sum_j a_j^{(k)} X_m^{\pm(j)} \tag{24}$$

of the total energy. We may assume the $\{U^{(k)}\}$ have norm R^2 in the sense of Eq. (16) where R is the unit of length. The eigenvalues $\lambda_{km}^\pm$ are generalized Hooke's law constants. Explicit formulas for $E_m^{\pm ij}$ are given in Appendix D. It is noteworthy that all rigid motions of M emerge as null vectors of this procedure, a good computational check.

One also finds that not all stationary shapes of E_{tot} are infinitesimally stable. Since long-term stability is apparently determined by E_B alone, it is enough to consider the case $\mu = 0$. If c_0 is too positive, an eigenvalue becomes negative, which corresponds to an unstable mode which is approximately Y_{22}. If c_0 is too negative, an eigenvalue becomes negative, which corresponds to an unstable mode that is approximately Y_{30}. These infinitesimal instabilities occur whether the BCH is true or not. Observed instabilities of the red-blood-cell shape (leading to sickle cells on the one hand and stomatocytes on the other) may be manifestations of these instabilities. The situation is illustrated in Fig. 2. Even for shapes that are infinitesimally stable, these two modes are soft if $\mu = 0$, a result that has observable consequences in flicker (thermal shape fluctuations).

If μ is large, in the sense that the shear energy dominates the deformation energy, the character of the nor-

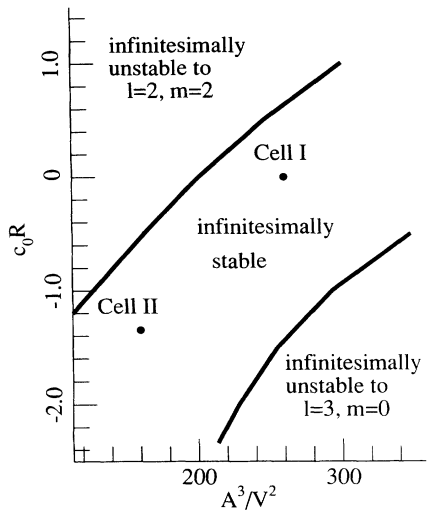

FIG. 2. The normal discocytic equilibrium shape of the erythrocyte is infinitesimally stable only in the indicated part of parameter space. The two model cells used for computations in this paper are indicated. Cell I is shown in Fig. 1.

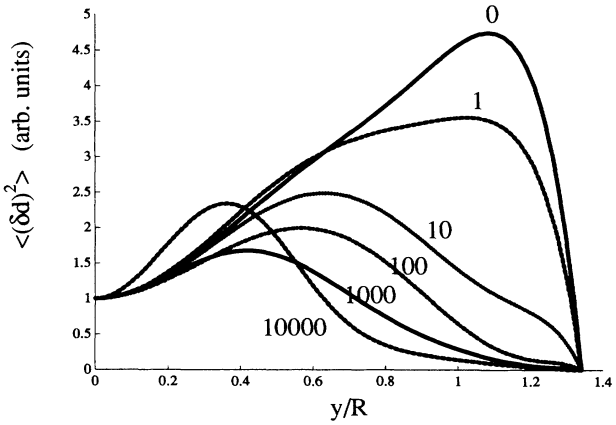

FIG. 3. Thickness fluctuation profile for various values of the ratio $\mu R^2/k_c$, indicated next to each curve. The effect of increasing this ratio is to move the peak in thickness fluctuations toward the center of the cell ($y=0$). For $\mu=0$ (fluid membrane) the peak is near the rim of the cell.

mal modes is quite different. They do not resemble spherical harmonics, and the softest mode (apart from the zero-energy Euclidean motions) is an $m=1$ mode that is even in inversion (odd in equatorial plane reflection). It is possible that this mode may be seen in tank-treading experiments (see Fig. 16).

V. FLICKER AMPLITUDES

The mean-square displacement of M in thermal shape fluctuations is, by the equipartition theorem,

$$\langle |\delta X(s)|^2 \rangle = \sum_{m,k} \frac{k_B T}{\lambda_m^{\pm(k)}} |U_m^{\pm(k)}(s,\psi)|^2 , \tag{25}$$

where the sum goes over both even and odd modes, but omits the rigid motions. What is usually observed is the fluctuation in thickness along the direction of the rotation axis, namely

$$d(s,\psi)=2x(s)+[N(s,\psi)-N(\pi-s,\psi)]\sin(\Theta(s)) , \tag{26}$$

for which the equipartition theorem predicts

$$\langle |\delta d(s)|^2 \rangle = 4 \sum_{m,k} \frac{k_B T}{\lambda_m^{+(k)}} |\hat{n}\cdot U_m^{+(k)}(s,\psi)|^2 \sin^2(\Theta(s)) . \tag{27}$$

Here the superscript + means "even" in equatorial reflection, not inversion. The Euclidean rigid modes are of course omitted from the sum.

Figure 3 shows $\langle |\delta d(s)|^2 \rangle$ vs $y(s)$ for several values of μ. All curves are normalized to 1 at $s=0$ (center of the cell). The influence of μ on the normal modes is clearly visible. Increasing μ suppresses the soft Y_{22} peak, which is responsible for most of the $\mu=0$ profile. The relatively low profile in the center, for all values of μ, is a result of the global constraints, which essentially remove the lowest two $m=0$ modes. The BCH, which removes a third mode, makes a noticeable difference, as shown in Fig. 4.

Recent data indicate that the flicker amplitude follows the $\mu=0$ profile, and respects the BCH [22]. This is a surprise, because other experiments, including the micropipette experiments, certainly indicate a large value for μ. On the other hand, a large value for μ would make flicker amplitudes unobservably small in any case. Flicker seems to be the motion of the fluid bilayer component, in which the cytoskeleton, with its shear modulus, somehow is not seen.

The recent measured values of flicker amplitudes are considerably smaller than what has been reported in the past, and the implied value for the bending modulus k_c is larger. It seems quite certain that the root-mean-square

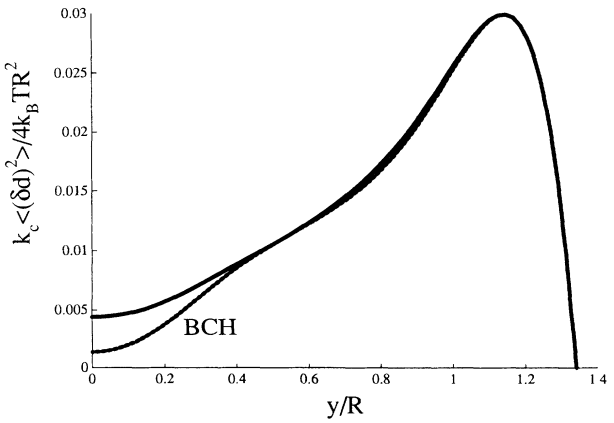

FIG. 4. Thickness fluctuations profiles with and without the bilayer coupling hypothesis (BCH). The BCH constraint essentially removes one $M=0$ fluctuation mode.

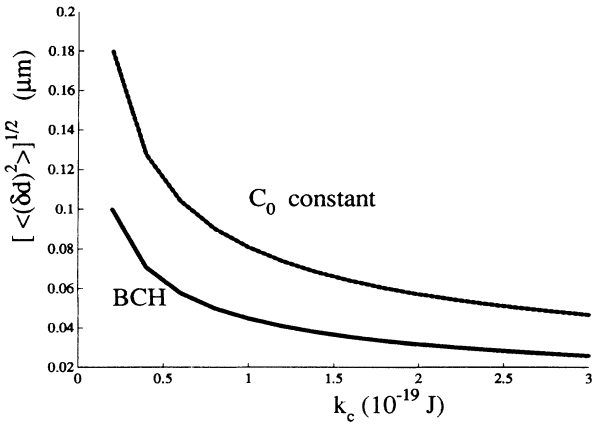

FIG. 5. The predicted root-mean-square thickness-fluctuation amplitude at $T=293$ K in the center of the erythrocyte is shown as a function of the bending modulus k_c both with and without the BCH.

amplitude in the center must be much smaller than the value obtained by Brochard and Lennon [10] (about 0.08 μm) if the profile follows Fig. 4, because the amplitude near the rim of the cell would be unacceptably large, easily visible as a fluctuating cell outline in the microscope. The amplitude seems to be more nearly 0.03 μm in the center of the cell, giving a value for the bending modulus k_c of $2-3\times10^{-19}$ J, as one sees in Fig. 5. This value for k_c is typical of artificial lipid bilayers [23,24,25].

If the rms thickness fluctuation in the center is 0.03 μm, the rms normal fluctuation amplitude at the rim of the cell is about 0.11 μm if the BCH is true and 0.06 μm if c_0 is constant. The accompanying (dimensionless) shear strain is highest at the rim, about 4% with the BCH, and 2% if c_0 is constant. This shear strain appears not to cost elastic energy. To repeat, flicker looks like the motion of a fluid membrane. It is not plausible that the fluid moves independently of the cytoskeleton, since the amplitude of the normal motion is quite large. Alternatively the cytoskeleton may be loose somehow, so that small strains, up to a few percent, create no stress.

VI. ELECTRODEFORMATION

An erythrocyte in a high-frequency electric field (1 MHz) of around 30 000 V/m is appreciably stretched [12]. It is possible to suspend the erythrocyte in a sugar solution of low conductivity, so that the problem is approximately the electrostatics problem of a perfect conductor (the cell) in a dielectric (the suspending medium). The boundary conditions are particularly simple in this case: M is an equipotential surface. The method of this section can be extended to the case of finite conductivity ratio (cytoplasm to suspending medium), which changes the boundary condition slightly. However, Grebe has emphasized that the membrane contains mobile, charged molecular species, and so ought to be considered a two-dimensional conductor, and an equipotential surface, even in this case [26].

I adopt the following algorithm: (i) Solve Maxwell's equations (really just the Laplace equation, in the simplest case) outside and inside the cell, subject to boundary conditions, for fixed shape (initially the equilibrium shape); (ii) use the solution to compute the stress on the cell; and (iii) use the normal modes $\{U^{(k)}\}$ to determine the shape response of the cell to this stress.

In principle, one can now repeat these steps, going back to step (i) with the new shape, finding the (small) correction to the fields, the stress, etc., and in this way develop a power-series solution, which would certainly converge for small applied field. If one stops at step (iii), though, one has already correctly computed the linear term.

The geometry of the experiment is shown in Fig. 6. The electric field outside the cell is determined by a potential

$$\Phi(X,Y,Z)=Y+\phi(X,Y,Z)\ , \tag{28}$$

where

$$\begin{aligned}&\nabla^2\phi=0\ \text{(outside } M)\ ,\\ &\phi|_M=-y(s)\cos(\psi)=-\mathrm{Re}[y(s)e^{i\psi}]\ .\end{aligned} \tag{29}$$

To solve Eq. (29) in a practical sense one needs a flexible family of functions harmonic outside M with $m=1$ symmetry. This is provided by the potential of charged rings in the equatorial plane, centered on the origin, having radius a less than the radius of the cell, and with charge distribution $e^{i\psi}$:

$$\phi_a(s,0)=\int_0^{2\pi}e^{i\beta}[x^2+y^2-2ay\cos(\beta)+a^2]^{-1/2}d\beta\ . \tag{30}$$

In Eq. (30) I have computed this function on M at $\psi=0$ (i.e., on the curve C), which is all one really needs. In group-theoretical language one is projecting the $m=1$ representation from the reducible representation of a point charge located a distance a off center.

Now I find coefficients b_k corresponding to ring radii a_k such that

$$\sum_k b_k\phi_{a_k}(s)=-y(s)\ . \tag{31}$$

The coefficients b_k determine the charges on the rings, which give the potential ϕ outside M. In practice it is enough to tabulate ϕ_a for ten or so uniformly spaced

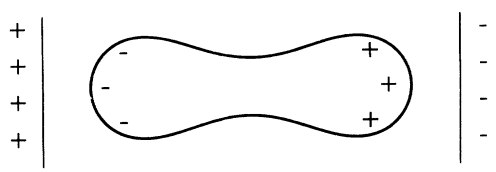

FIG. 6. An erythrocyte in an electric field polarizes and is distorted. (Electrodes may actually be many cell diameters apart.)

rings and to solve Eq. (31) in the sense of least squares. One easily finds ϕ, and hence Φ, to four-place accuracy.

The corresponding normal component of the (dimensionless) electric field

$$E_n = -\frac{\partial \Phi}{\partial n} , \tag{32}$$

shown in Fig. 7, also belongs to $m=1$. The Maxwell stress, proportional to E_n^2, belongs to $m=0$ and 2, parity even. Representing it as a linear combination of normal modes,

$$\tfrac{1}{2}E_n^2(s) = \sum_k c_0^k U_0^{+(k)}(s,0) , \tag{33}$$

$$\tfrac{1}{2}E_n^2(s) = \sum_k c_2^k U_2^{+(k)}(s,0) , \tag{34}$$

I find, putting all dimensional factors in, the displacement of M,

$$X(s,\psi) = \frac{R}{2}\epsilon\langle E^2\rangle \sum_k (d_0^k U_0^{+(k)} + d_2^k U_2^{+(k)}\cos 2\psi) , \tag{35}$$

where

$$d_0^k = c_0^k/\lambda_0^{+(k)} , \tag{36}$$

$$d_2^k = c_2^k/\lambda_2^{+(k)} , \tag{37}$$

and $\langle E^2\rangle = \frac{1}{2}E_{\max}^2$ is the mean-square amplitude of the high-frequency field.

In Figs. 8 and 9 are the predicted shapes for $\mu=0$ and $1000k_c/R^2$, respectively. For large μ the field produces "ridges" parallel to the field, with a long valley between them. For small μ the ridges are replaced by a high rim at the front and back of the stretched cell, with saddle points on the rim at 90° to the field. Observed shapes look like Fig. 9 [27]. That is, the evidence of the shape is that the important energy term is indeed a shear energy, not a curvature energy.

In an inhomogeneous field, the potential Φ on M is a linear combination of contributions from several symmetry classes. The problem for Φ can be solved in each symmetry class separately, the results superposed, etc. The predicted shape for an erythrocyte near a razor-blade electrode is shown in Fig. 10, where the inhomogeneous field has pulled the "ridges" into the stronger field region.

The predicted elongation response to the field E, for small E, is shown in Fig. 11 for various assumptions about the elastic moduli k_c and μ. This quantity has been measured by Kage and Sackmann [28]. The electrodes were $d=0.127$-mm-diam platinum wires in a flow chamber of internal width 2 mm, so that the center-to-center distance of the wires was $2a=1.873$ mm. The nearly homogeneous field in the center of the chamber is, in first approximation,

$$E = \frac{V}{a\ln(4a/d)} , \tag{38}$$

if V is the applied voltage difference. It is observed that a

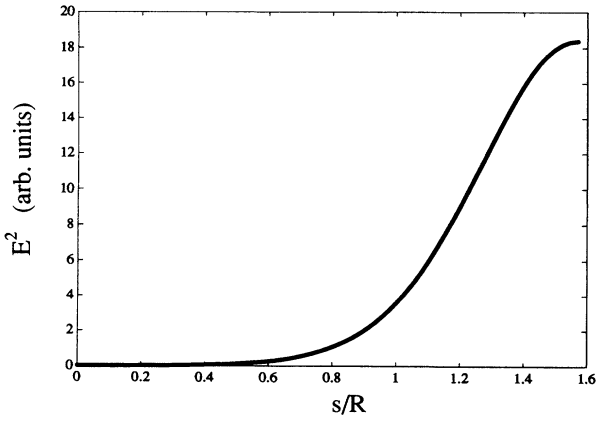

FIG. 7. The squared normal component of an electric field on the curve C if the cell is an equipotential.

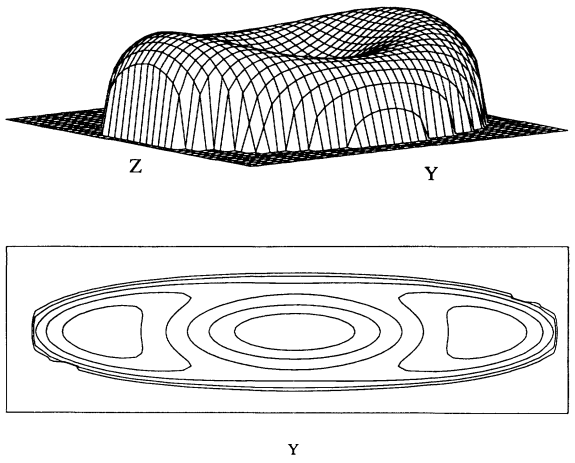

FIG. 8. Predicted shape for erythrocyte in a homogeneous electric field if the membrane is fluid.

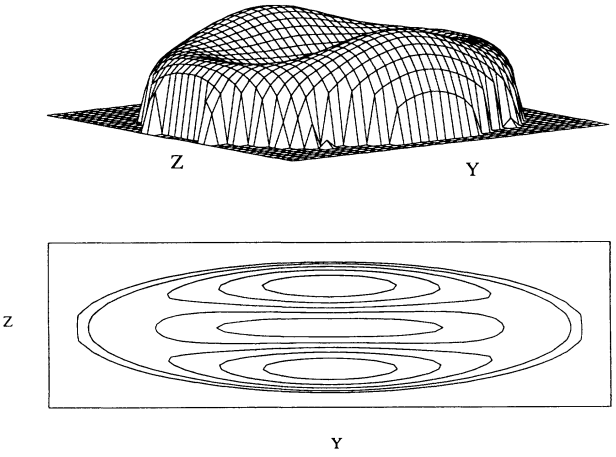

FIG. 9. Predicted shape for erythrocyte in a homogeneous electric field if $\mu R^2 = 1000k_c$.

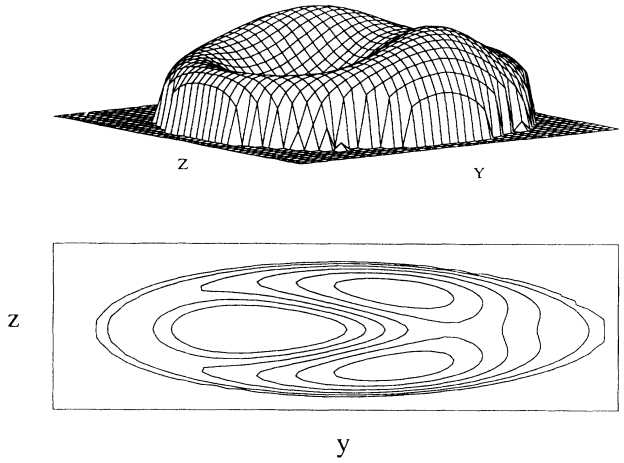

FIG. 10. Predicted shape for erythrocyte in an inhomogeneous field near a razor edge if $\mu R^2 = 1000 k_c$. In the contour plot, the electrode is on the right.

1-MHz field with amplitude of 50 V produces a lengthening of the semimajor axis $\Delta y = 1.8\mu$, and that the lengthening is linear in voltage squared, as expected. Using $\epsilon = 80\epsilon_0$, for the dielectric property of the suspending solution, one finds the value $0.049 \times 10^{19}\ \mathrm{J}^{-1}$ for the combination of experimental quantities graphed in Fig. 11. If k_c is $2-3 \times 10^{-19}$ J, as indicated by the flicker amplitudes, μ must be about 1×10^{-6} N/m, which is much less than the standard value $6-9 \times 10^{-6}$ N/m determined in micropipette aspiration [2].

VII. FLOWS

Analysis of tank treading and flicker relaxation modes requires matching of the membrane motion to Stokes flows inside and outside M. For this purpose one needs flows (vector fields) V or equivalently 1-forms $\tilde{V}$ and corresponding (scalar) pressure fields P satisfying

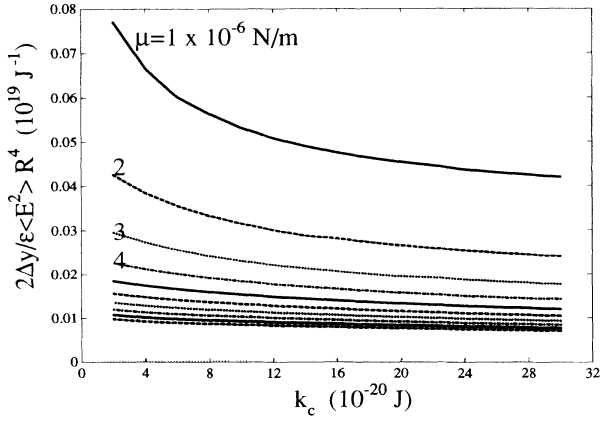

FIG. 11. Predicted elongation in the electric field E for various values of the elastic constants. $2\Delta y$ is the elongation of the diameter, and $\epsilon = 80\epsilon_0$ is the dielectric permittivity of water. The quantity on the abscissa is a purely experimental number and has a value about $0.05 \times 10^{19}\ \mathrm{J}^{-1}$.

$$\begin{aligned} d * \tilde{V} &= 0 \ , \\ dP + \eta * d * d\tilde{V} &= 0 \ . \end{aligned} \tag{39}$$

Here η is the viscosity of the fluid. The three-dimensional shear strain S of a flow V is [29]

$$S = \tfrac{1}{2}\mathcal{L}_V G \ , \tag{40}$$

where $\mathcal{L}_V$ means the Lie derivative with respect to the flow V, and G is the metric tensor. Elementary flows which are useful in problems of this type are familiar from textbooks.

To exploit the symmetry of this problem I project flows with the same symmetry as the membrane normal modes. A compact way to express the rotation symmetry of the normal modes is

$$\mathcal{L}_R U_m = im U_m \ , \tag{41}$$

where R is the vector field which generates rigid rotations about the x axis. Thus the symmetric flows are

$$V_m^{\pm} = \frac{1 \pm P}{2} \int_0^{2\pi} e^{im\beta} e^{-\beta \mathcal{L}_R} V d\beta \ , \tag{42}$$

where P is the reflection operator. This formula is a kind of analog of Eq. (30). More explicit versions of this formula are in Appendix E.

By construction

$$\mathcal{L}_R V_m^{\pm} = im V_m^{\pm} \ . \tag{43}$$

The corresponding shear strain tensor S has the same behavior, because

$$\begin{aligned} 2\mathcal{L}_R S &= \mathcal{L}_R \mathcal{L}_V G \\ &= (\mathcal{L}_R \mathcal{L}_V - \mathcal{L}_V \mathcal{L}_R) G \\ &= \mathcal{L}_{[R,V]} G \\ &= \mathcal{L}_{imV} G \\ &= im \mathcal{L}_V G \\ &= 2imS \ . \end{aligned} \tag{44}$$

This means that in the (n,s,ψ) coordinate basis, the effect of rotation is simply to multiply each component of V and S by $e^{im\psi}$. Since all vector fields and tensor fields have been constructed to have the same behavior, it is enough in linear boundary value problems to match them along the curve C within each symmetry class, as we did in Eqs. (33) and (34).

VIII. TANK TREADING

An erythrocyte in a shear flow takes up a stationary orientation with respect to the flow, and the membrane "tank treads" around the interior cytoplasm at a definite frequency ν (proportional to the external shear rate $\dot{\gamma}$). It also elongates. It is necessary for the external viscosity to be sufficiently large—otherwise the cell tumbles in the flow instead of smoothly tank treading [14]. The situation is illustrated in Fig. 12.

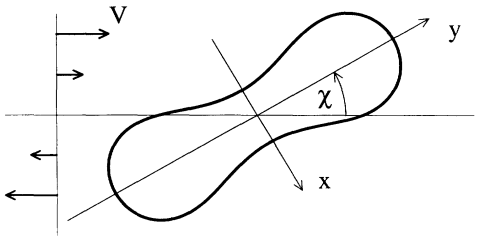

FIG. 12. Geometry of tank treading. The cell tilts at a stationary angle χ in the shear flow V.

I adopt essentially the same approach as in electrodeformation.

(a) Solve for Stokes flows outside and inside M, which match the purely tangential constrained flow in M, such that tangential stresses also balance, and such that at large distances from the erythrocyte one has uniform planar shear flow. Do this for the equilibrium shape oriented at angle χ to the flow.

(b) Use the solution from (i) to determine the net torque on the cell, and repeat step (i), changing χ, until the net torque is zero, if this is possible. (For some choices of viscosities there is no such steady-state solution.)

(c) Use the normal stress from the steady-state solution and the normal modes of the membrane to find the new shape.

In principle one could go back to step (i) with the perturbed shape, etc., and find a power-series solution in powers of the shear rate, but I stop at the linear term.

The experimental existence of smooth tank treading, even at quite low shear rate, means that the relatively large membrane shear modulus μ is not important in step (i). The motion of the "dimple" around the cell would produce an oscillatory tangential stress for which there is no observational evidence once tank treading begins. I do include the membrane shear viscosity η_M in step (i), however. Details of the solution are in Appendix F.

In agreement with analytical solutions for ellipsoidal cells [30], I find a bifurcation from tumbling to tank treading as the viscosity η_{out} of the external medium increases. The threshold viscosity depends on the cell volume, η_{in}, and η_M. The behavior of the stationary angle χ is shown in Fig. 13 for a normal cell (cell I), and a somewhat swollen cell (cell II). The stationary angle is zero at threshold and increases with η_{out}. It is interesting to notice that in the swollen cell, in which the dimple is very shallow, the dependence on η_M is weak, while in the normal cell, even a very small η_M has a noticeable effect. This is undoubtedly because of the larger shear strain in the flow through the deep dimple in the normal shape. From the observed threshold value of $\eta_{\text{out}}/\eta_{\text{in}}$, which is about 0.8 for normal cells, one can see that

$$\eta_M \approx 0.3\eta_{\text{in}}R \ . \tag{45}$$

This is much smaller than the value $\eta_M \approx 50\eta_{\text{in}}R$ inferred from shape recovery in *all* experiments in which the cell is deformed and then released [2,12]. The simplest interpretation of this surprising result is that one is seeing the flow of the fluid component only, which has a fairly low viscosity.

A second effect permits an independent estimate of the membrane viscosity, and gives the same surprisingly low value. From the stationary solution one can find the period P for a point on the center line, and hence the frequency $\nu = 1/P$, which is of course predicted to be linear in shear rate $\dot{\gamma}$. Figure 14 shows $\nu/\dot{\gamma}$ for the same parameter values as Fig. 13. The more swollen cell has a higher frequency because it is exposed to higher speed in the shear flow. Again the normal cell values are quite sensitive to η_M. Values measured by Fischer and Schmid-Schoenbein, as estimated from their published graph [14], are indicated, and confirm the value of η_M

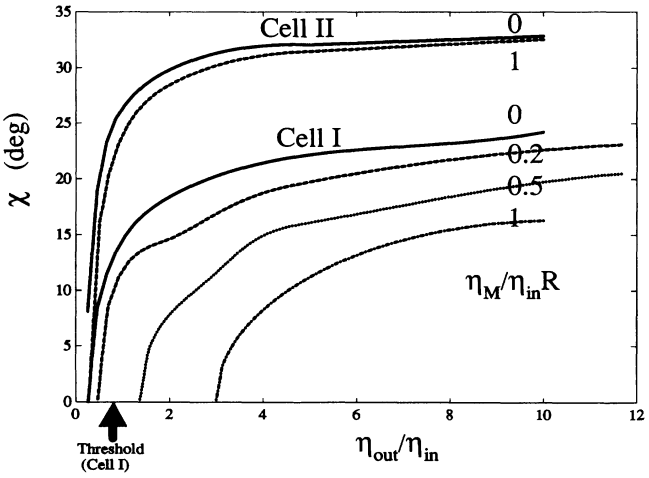

FIG. 13. Stationary angle χ for tank treading, as a function of the viscosities, for two different cell shapes, a normal cell (cell I), and a somewhat dilated cell (cell II). The experimental value of η_{out} at which normal cells begin tank treading is indicated by an arrow.

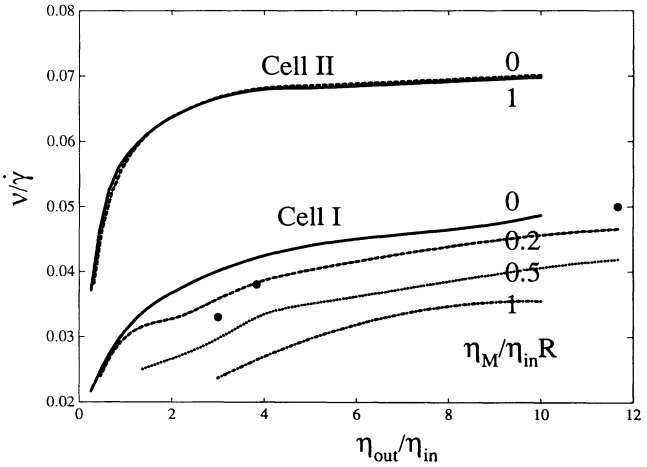

FIG. 14. Frequency $\nu/\dot{\gamma}$ for tank treading, as a function of the viscosities for two different cell shapes. The dots are experimental frequencies estimated from graphs published in Ref. [13].

found above. These two *independent* determinations of η_M agree remarkably. That even a small shear force disrupts tank treading in normal cells further justifies our claim above that the relatively large shear modulus μ could not play a role in tank treading.

Two puzzles are cleared up by the above analysis. Previous analysis of tank treading, using a liquid-drop model [31], led to qualitative agreement with experiment and established that the cell interior is fluid. In that analysis, however, the tank-treading frequency (at fixed shear rate $\dot{\gamma}$) *decreases* with increasing external viscosity, contrary to what is observed. It is clear in Fig. 14 that the frequency should increase slightly, as the experiments show. In addition, the elongation of the cell is observed to be a universal function not of the naive applied stress $\eta_{\text{out}}\dot{\gamma}$, as the liquid-drop analysis predicts, but of the combination $\eta_{\text{out}}^{1.7}\dot{\gamma}$, where the exponent 1.7 is found empirically [32]. The reason for that is that the stationary angle χ increases with increasing η_{out} (see Fig. 13). The elongation stress, which is effectively in the $m=2$ symmetry class, is proportional to $\eta_{\text{out}}\dot{\gamma}\sin 2\chi$ (see Appendix F). It is the increase in $\sin 2\chi$ which is being noticed. The nonlinearity can be traced back to the zero torque condition, a nonlinear equation for the parameters of the flow. Thus, even without a detailed analysis of elongation, one can see that there will be an effect of the kind observed. A fit to the analysis below predicts an exponent of about 1.4 over the viscosity range used in the experiments, rather than 1.7. The experimental data are largely at shear rates outside the linear regime, however, so that full quantitative agreement is not be expected.

In the elongation of the cell it is clear that the solid component plays a role, by the large elastic modulus that is indicated. Most published data are at shear rates outside the linear regime, but in Ref. [14] one can see the linear increase in ellipticity $(L-B)/(L+B)$ for a normal cell in a medium of viscosity 23 cP, which is about $0.005\dot{\gamma}$ (where $\dot{\gamma}$ is in sec^{-1}). This cell is also well

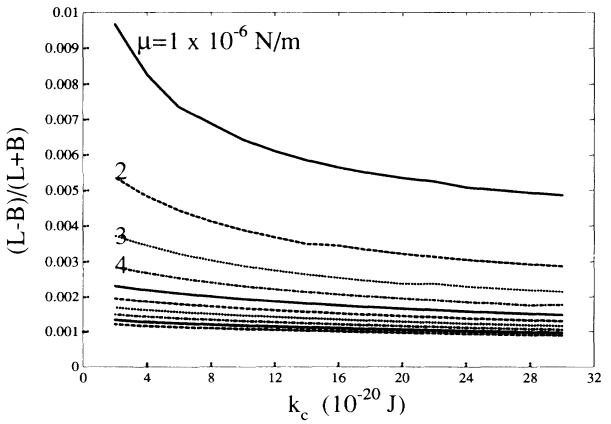

FIG. 15. Ellipticity $(L-B)/(L+B)$ at unit shear rate $\dot{\gamma}$ in tank treading for a normal cell in a medium with viscosity 23 cP. Here L means length and B means breadth of the elliptical shape seen in vertical projection in the rheoscope. The experimental value is about 0.005, as estimated from the graph published in Ref. [13].

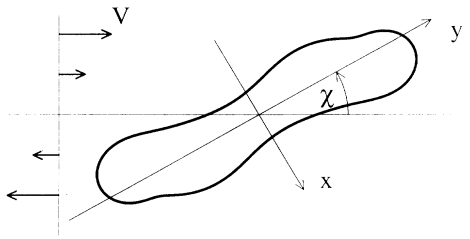

FIG. 16. A side view of the predicted erythrocyte shape in tank treading.

characterized by the steady-state solution above, so that the stresses are accurately known. Figure 15 shows the expected ellipticity for various assumptions about the elastic moduli k_c and μ. It is clear that μ as determined in this way is the same order of magnitude as that found in the electrodeformation experiment, 1×10^{-6} N/m, much smaller than the value obtained in micropipette experiments ($6-9\times10^{-6}$ N/m).

Using the computed normal stress of the exterior fluid, and the normal modes of the membrane, I determine the perturbed shape shown in Fig. 16. The predicted normal shape is "bent" by the shear flow. This "side view" in tank treading is not yet accessible experimentally.

IX. FLICKER RELAXATION MODES

Finding the hydrodynamic relaxation modes of erythrocyte flicker is a generalized eigenvalue problem. It has been solved in the spherical limit in Ref. [33], and the solution using the actual shape is quite close to the spherical limit, as one sees by the decay rates in Table I. These were obtained by matching the flows inside and outside the cell, and the motion of the membrane itself, just as in the other sections of this paper. Solutions were sought with time dependence $e^{-\Gamma t}$. Thus, schematically, if A is the amplitude of the membrane distortion, its velocity should be $-\Gamma A$. Membrane stresses can be computed from A and $-\Gamma A$. Then the condition that all velocities should match on the membrane, and that all stresses should balance, is a large homogeneous linear problem, in which Γ occurs as a multiplier in some terms, i.e., a generalized eigenvalue problem, where Γ is the eigenvalue. The corresponding eigenvector is the hydrodynamic mode, representing the motion of interior and exterior fluids, and the membrane, in the bases we have chosen.

In solving this problem one must explicitly include the stresses which maintain the constraints. Thus, for example, corresponding to the volume constraint, one must allow for a nonequilibrium hydrostatic pressure difference between inside and outside. Since it is part of the mode, this pressure difference decays with the rate Γ, just as everything else does. The local incompressibility of the membrane requires that there be the gradient of a two-dimensional pressure in the tangential stress, just as in Eq. (140), etc. Without these terms there is no solution to the boundary-value problem. (It is also necessary to al-

TABLE I. Hydrodynamic thickness mode relaxation rates in sec^{-1} for cell II. The computation assumes $k_c = 2.4 \times 10^{-19}$ J, $\eta_{out} = 1$ cP, and $\eta_{in} = 4$ cP. Spherical limit values are given for comparison, with their corresponding l's. Only modes which are even in equatorial reflection are shown. The shapes of these modes can be seen in Fig. 17.

$m=0$	$m=1$	$m=2$	$m=3$	Parity	Spherical limit	
		0.84		even	0	$l=2$
	8.56		5.88	odd	13.50	$l=3$
37.4		39.22		even	41.42	$l=4$
	94.2		81.26	odd	87.8	$l=5$
174.2		172.2		even	157.4	$l=6$

low a completely general motion of the membrane, subject only to the constraints: in the spherical limit the normal motion with its accompanying induced tangential flow $d\alpha$ decouples from the tangential flow $*d\beta$, but in the general problem they are coupled.) Corresponding to the experiments described in Ref. [22], the cell was constrained not to translate by eliminating the Euclidean translation mode from the space of allowed motions and including a stress conjugate to translation to enforce the constraint. (In the experiment, the cell is lightly attached to the substrate at one point.)

The hydrodynamic modes, considered as modes of the membrane, do not coincide with the energy eigenmodes. Thus the energy eigenmodes, which are excited with mean-square amplitudes given by the equipartition theorem, as in Sec. V, relax, on average, according to hydrodynamics, that is, as a linear combination of hydrodynamic modes. Figure 17 shows the decomposition

$$\langle \delta d(y,0)\delta d(y,t)\rangle = \sum_i H_i(y) e^{-\Gamma_i t} \tag{46}$$

of the mean-square thickness-fluctuation profile of Fig. 4 into decaying modes. The only noticeable effect of the BCH is to eliminate the largest $M=0$ mode. The small membrane viscosity η_M indicated in the tank-treading experiments has negligible effect on the decay rates. There are only a few important shape decay modes. Their discrete rates are well separated, and their rotational symmetry and radial dependence should make it possible to distinguish them experimentally. Although this separation has not been done yet experimentally, the decay times which are present with appreciable amplitude in the correlation functions are similar to those in Fig. 17, which is additional support for the value of k_c found from the mean-square amplitudes alone.

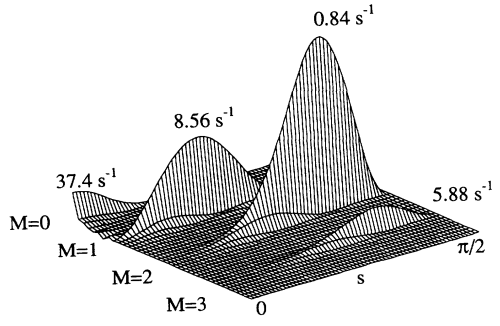

FIG. 17. Hydrodynamic thickness fluctuation modes, with indicated rotational symmetry M. The $M=0$ modes contribute predominantly near the center of the cell, $s=0$. The rim of the cell is at $\pi/2$.

X. CONCLUSION

Assuming that the elastic energy of the membrane is given by Eqs. (17) and (18), I have solved linear boundary-value problems which describe flicker, electrode formation, and tank treading of erythrocytes, three methods for observing the linear response of the erythrocyte to mechanical stress. The results of these computations can be used to interpret existing data. These experiments are consistent in indicating a fluid component with a bending modulus $k_c \approx 3 \times 10^{-19}$ J and two-dimensional shear viscosity $\eta_M \approx 5 \times 10^{-9}$ N s/m, and a solid component with a shear modulus $\mu \approx 1 \times 10^{-6}$ N/m and a two-dimensional shear viscosity $\eta_S \approx 10^{-7}$ N s/m. k_c is determined in flicker in two independent ways, by the mean-square amplitude and by the decay rates. η_M is determined in two independent ways in tank treading, by the tank-treading threshold and by the observed tank-treading frequencies. Its smallness is corroborated by the flicker decay rates. μ is determined in electrodeformation and in the elongation response in tank treading. Finally η_S, the viscosity of the solid component, is determined by the characteristic shape recovery time in electrodeformation and tank treading when the deforming stress is removed, about 0.1 sec [2]. It is worth noting that only the tank-treading experiments show both fluid and solid properties simultaneously. Flicker shows only fluid properties and electrodeformation shows only solid properties.

A remarkable recent experiment by Weaver *et al.* [34] on diffusion of the membrane protein ankyrin during tank treading indicates that the diffusion is unaffected by the overall motion of the membrane. This was interpreted to mean that both the lipid and the cytoskeleton move together, since differential motion of the two components might be expected to enhance diffusion. This picture of fluid and solid moving together is contrary to my analysis of tank treading, which indicates that only a fluid membrane tank treads, but the ankyrin evidence is slightly indirect. Much more direct would be to watch fluorescently labeled spectrin during tank treading.

If it can be shown that the cytoskeleton does indeed flow around the cell during tank treading, one would

have to understand how it can do so without appreciable shear stress. The geometrical analysis of this paper has one suggestion to make in this case. The tangential flows which produce shear strain are uniquely decomposable into "α flows," of the form $d\alpha$, which are induced by shape change, and "β flows," of the form $*d\beta$. Although it is difficult to imagine a molecular mechanism, it is possible that the cytoskeleton responds like a solid only to α flows. Since the tank-treading flow is a β flow, it would induce no shear stress.

ACKNOWLEDGMENTS

I would like to thank Professor Erich Sackmann of TU-Muenchen and Professor Gisbert zu Putlitz of Universität Heidelberg for hospitality while much of this work was done. For helpful conversations and encouragement I thank Professor E. Sackmann, Professor W. Helfrich, Professor T. M. Fischer, Professor H. Schmid-Schoenbein, Helmut Strey, Hans Sixtus Kage, Joachim Raedler, and Andreas Zilker. This work was supported by a Faculty Research Grant from Mount Holyoke College.

APPENDIX A: GEOMETRICAL OPERATIONS

Let the indices (1,2) stand for the coordinate (s,ψ), and indicate partial differentiation and covariant differentiation by a coma and a semicolon, respectively. Then, if A^i is a vector field,

$$A^i_{;j}=A^i_{,j}+\Gamma^i_{jk}A^k \ , \tag{A1}$$

where

$$\Gamma^1_{22}=-y\sin\Theta \ , \qquad \Gamma^2_{12}=\Gamma^2_{21}=\frac{\sin\Theta}{y} \ , \tag{A2}$$

and all other Γ's are zero.

The Hodge star operator ($*$) maps 1-forms to 1-forms according to

$$*(ads+bd\psi)=\frac{b}{y}ds-ayd\psi \ . \tag{A3}$$

If

$$\tilde{X}_m=Ndn+ads+bd\psi \tag{A4}$$

is a 1-form on M belonging to symmetry class m, then the two-dimensional shear strain of the corresponding vector field X_m is

$$S_{11}=a_{,1}+Nc_1 \ , \qquad S_{12}=S_{21}=\tfrac{1}{2}(ima+b_{,1})-\frac{\sin\Theta}{y}b \ , \qquad S_{22}=imb+ay\sin\Theta+Ny^2c_2 \ . \tag{A5}$$

The orthogonal transformation from the (fixed) Cartesian frame to the orthonormal (n,s,ψ) coordinate frame is given by

$$\hat{n}=\hat{x}\sin\Theta-\hat{y}\cos\Theta\cos\psi-\hat{z}\cos\Theta\sin\psi \ , \qquad \hat{s}=\hat{x}\cos\Theta+\hat{y}\sin\Theta\cos\psi+\hat{z}\sin\Theta\sin\psi \ , \qquad \hat{\psi}=-\hat{y}\sin\psi+\hat{z}\cos\psi \ . \tag{A6}$$

APPENDIX B: BASIS VECTOR FIELDS

It is useful to find the matrix of the Laplace-Beltrami operator in each symmetry class:

$$\Delta^{(m)\pm}_{ll'}=-2\pi\int_0^\pi\left[\frac{d\bar{Y}_{lm}}{ds}\frac{dY_{l'm}}{ds}+\frac{m^2}{y^2}\bar{Y}_{lm}Y_{l'm}\right]yds \ , \tag{B1}$$

where l and l' are both even (+) or both odd (−). In practice one truncates this infinite matrix at some suitably high l, of course. Other useful matrices are

$$A_{ll'}=2\pi\int_0^\pi\bar{Y}_{lm}Y_{l'm}y\,ds \tag{B2}$$

and

$$H_{ll'}=2\pi\int_0^\pi\bar{Y}_{lm}HY_{l'm}y\,ds \ , \tag{B3}$$

where again one may restrict attention to one symmetry class at a time. For simplicity of notation I leave off the symmetry class labels $\pm$ and m in what follows.

Solve the generalized eigenvalue problem

$$\Delta Z=AZD \tag{B4}$$

for a square matrix Z and a diagonal matrix D, and normalize the columns of Z so that

$$Z^TAZ=I \ . \tag{B5}$$

The columns of Z are the eigenfunctions of Δ in the spherical harmonic basis. These functions provide an orthonormal basis in each symmetry class of $L^2(M)$, which I call the Z basis. In the symmetry class $l=$even,$m=0$, one must make an orthogonal change of basis to respect the integral constraints Eqs. (11), (12), and (13). One may do this by the Gram-Schmidt procedure, taking the functions 1, H, K, and the columns of Z after the third as a starting point. The resulting basis, which will be the columns of ZT, where T is an orthogonal matrix, will be called the *admissible* basis. In other symmetry classes T is the identity matrix. The normal component N of any deformation will be understood henceforth as a column vector, whose entries are the components of the function N in this admissible basis. The integral constraints then amount to requiring that the first two (or three) entries be zero.

The solution of Eq. (15) now is

$$\alpha(N)=-2ZD^{-1}Z^THZTN \ , \tag{B6}$$

where α is a column vector whose entries are the components of the function α in the spherical harmonic basis. If l is even and $m=0$, D^{-1} still makes sense provided the first two entries of N are zero.

Let e_i denote the column vector which is 1 in the ith place and zero elsewhere. Then

$$\tilde{X}_N^{(i)}=\sum_l (ZT)_{li}Y_{lm}dn+\alpha(e_i)_l dY_{lm} , \tag{B7}$$

$$\tilde{X}_\beta^{(l)}=*dY_{lm} , \tag{B8}$$

are 1-forms corresponding to displacements which obey all constraints. The corresponding vector fields $X_N^{(i)}$ change the shape, and the $X_\beta^{(i)}$ do not. Finally, choose a basis $\{X^{(i)}\}$ which diagonalizes the inner product Eq. (16) $(X_N^{(i)},X_N^{(j)})$ and $(X_\beta^{(i)},X_\beta^{(j)})$, and is normalized in the sense

$$(X^{(i)},X^{(j)})=R^4\delta_{ij} , \tag{B9}$$

where, for dimensional reasons, R is the unit of length (fixed by the condition that curve C have length $\pi/2$). In terms of this basis one needs the transformation

$$X_N^{(i)}=\sum_j O_N^{ij}X^{(j)} , \tag{B10}$$

$$X_\beta^{(i)}=\sum_j O_\beta^{ij}X^{(j)} \tag{B11}$$

when one expands the energy.

APPENDIX C: MODEL CELLS

Curve C giving an azimuthally symmetric stationary shape M of E_B can be generated as a solution of the Euler-Lagrange equations [35]

$$x'=\cos\Theta , \tag{C1}$$

$$y'=\sin\Theta , \tag{C2}$$

$$\Theta'=p , \tag{C3}$$

$$p'=\left[-\lambda y^2\sin\Theta-2p\sin\Theta-\frac{2\cos\Theta\sin\Theta}{y}-b\cos\Theta\right]\Big/2y , \tag{C4}$$

$$b'=2\lambda y\cos\Theta+\sigma+p^2-\frac{\cos^2\Theta}{y^2}-2c_0p , \tag{C5}$$

with initial data

$$x(0)=y(0)=p'(0)=b(0)=0 , \tag{C6}$$

$$\Theta(0)=\pi/2 , \tag{C7}$$

$$p(0)=p_0 , \tag{C8}$$

$$b'(0)=\sigma-2c_0p_0 . \tag{C9}$$

Here λ, σ, and c_0 may be regarded as Lagrange multipliers to control V, A, and $\langle H\rangle$. p_0 is a free parameter which must be chosen to make $b=0$ when $\Theta=\pi$ in order that M be smooth at the equator. Once the solution is found, one can translate it so that the origin of coordinates is at the center of inversion symmetry. Two (equivalent) dimensionless measures of distance from the spherical shape are given in Table II, the reduced volume

$$V/V_0=\left[\frac{36\pi V^2}{A^3}\right]^{1/2} \tag{C10}$$

TABLE II. Data for two model cells, including parameters necessary to generate them using the differential equations of Appendix C. Cell I is shown in Fig. 1.

	Cell I	Cell II
Osmolarity	290 mOs	200 mOs
λ	−11.965 21	−11.950 45
σ	−8.573 66	−13.513 87
c_0	0	−1.385 15
p_0	−0.860 52	−0.305 01
V	3.542 7	4.472 3
A	14.832 6	14.736 4
$\langle H\rangle$	0.957 1	0.950 7
V/V_0	0.659 5	0.840 7
I_S	0.757 7	0.890 8
R	3.017 μm	3.027 μm

and the sphericity index

$$I_S=(V/V_0)^{2/3} . \tag{C11}$$

Both of these are 1 if the shape is a sphere. Dimensional measures are in units such that the length of curve C is $\pi/2$. R is the value of this unit of length in case the actual area is 135 μm^2, typical for an erythrocyte.

APPENDIX D: ENERGY EXPANSIONS

The second variation of E_B at fixed V, A, and c_0 for an admissible normal motion N, using the geometric data of Eqs. (3)–(8), is [29]

$$\delta^2E_B=\frac{k_c}{2}\int_M[(\Delta N)^2+A^{ij}N_{,i}N_{,j}+BN^2]dA , \tag{D1}$$

where

$$A^{ij}=-2(2H-c_0)(L^{ij}-Hg^{ij})+g^{ij}(-6H^2+4K-2c_0H+c_0^2/2+UP^{-1}V^{ij}) , \tag{D2}$$

$$B=16H^4-20H^2K+4K^2+2\Delta(2H^2-K)+4[(L^{ij}-Hg^{ij})H_{,i}]_{;j}+c_0^2K+UP^{-1}V , \tag{D3}$$

and where

$$U=[\langle -8H^3+4K(2H-c_0)\rangle,\langle 4|\nabla H|^2-8H^4+4HK(2H-c_0)\rangle] , \tag{D4}$$

$$P=\begin{bmatrix}1 & \langle H\rangle\\ \langle H\rangle & \langle H^2\rangle\end{bmatrix} , \tag{D5}$$

$$V^{11}=(0,-1/4)^T ,$$

$$V^{22}=(0,-1/4)^T , \tag{D6}$$

$$V^{12}=V^{21}=0 ,$$

$$V=(-H,-K/2)^T . \tag{D7}$$

The expansion of E_B at fixed V, A, and $\langle H \rangle$ (i.e., under the BCH) has the same form, but now

$$A^{ij} = -4HL^{ij} + g^{ij}(-2H^2 + 4K + UP^{-1}V^{ij}) , \tag{D8}$$

$$B = 16H^4 - 20H^2K + 4K^2 + 2\Delta(2H^2 - K) + 4[(L^{ij} - Hg^{ij})H_{,i}]_{;j} + UP^{-1}V , \tag{D9}$$

where now

$$U = (\langle -8H^3 + 8HK \rangle, \langle 4|\nabla H|^2 - 8H^4 + 8H^2K \rangle, \langle 4\nabla K \cdot \nabla H - 8H^3K + 8HK^2 \rangle) \tag{D10}$$

$$P = \begin{bmatrix} 1 & \langle H \rangle & \langle HK \rangle \\ \langle H \rangle & \langle H^2 \rangle & \langle K \rangle \\ \langle HK \rangle & \langle K \rangle & \langle K^2 \rangle \end{bmatrix} , \tag{D11}$$

$$V^{11} = (0 - 1/4, -c_2/2)^T ,$$

$$V^{22} = (0, -1/4, -c_1/2)^T , \tag{D12}$$

$$V^{12} = V^{21} = 0 ,$$

$$V = (-H, -K/2, 0)^T . \tag{D13}$$

In either case the matrix of $\delta^2 E_B$ in the basis of Eq. (61) is

$$E_B^{(2)} = O_N^T T^T (D^2 + Z^T Q Z) T O_N , \tag{D14}$$

where

$$Q_{ll'} = 2\pi \int_0^\pi \left[A^{11} \frac{d\bar{Y}_{lm}}{ds} \frac{dY_{l'm}}{ds} + (m^2 A^{22} + B) \bar{Y}_{lm} Y_{l'm} \right] y ds . \tag{D15}$$

The shear energy E_S is already a quadratic form in deformations. We have only to express it as a matrix in the orthonormal basis. The shear of the flow $X_N^{(j)}$ is

$$S_{11} = \sum_l \left[\frac{d^2 Y_{lm}}{ds^2} \alpha(e_j)_l + c_1 Y_{lm} (ZT)_{lj} \right] , \tag{D16}$$

$$S_{12} = S_{21} = \sum_l \left[im \frac{dY_{lm}}{ds} - im \frac{\sin\Theta}{y} Y_{lm} \right] \alpha(e_j)_l , \tag{D17}$$

$$S_{22} = \sum_l \left[\left[-m^2 Y_{lm} + y \sin\Theta \frac{dY_{lm}}{ds} \right] \alpha(e_j)_l + c_2 y^2 Y_{lm} (ZT)_{l_j} \right] . \tag{D18}$$

The shear of the flow X_β^l is

$$S_{11} = \frac{im}{y} \left[\frac{\sin\Theta}{y} Y_{lm} - \frac{dY_{lm}}{ds} \right] , \tag{D19}$$

$$S_{12} = S_{21} = \frac{1}{2} \left[\frac{m^2}{y} Y_{lm} - \sin\Theta \frac{dY_{lm}}{ds} + y \frac{d^2 Y_{lm}}{ds^2} \right] , \tag{D20}$$

$$S_{22} = imy \left[\frac{dY_{lm}}{ds} - \frac{\sin\Theta}{y} Y_{lm} \right] . \tag{D21}$$

With Eqs. (62) and (63) one can find the shear of $X^{(i)}$, and putting these expressions into Eq. (18) one finds the matrix elements as definite integrals involving spherical harmonics and geometric data of M. Of course one can do all this within each symmetry class, but note that the Hodge star operation reverses parity.

APPENDIX E: SYMMETRIC STOKES FLOWS

Elementary solutions of the Stokes equations Eq. (39) have a singularity at a point and a distinguished axis. If one takes such a solution with its singularity *not* at the origin, and rotates it rigidly about the x axis, one can, by superposition, create solutions which are singular on rings and have definite rotation symmetry in the sense of Eq. (43). This is the meaning of Eq. (42). The associated shear strain tensor and pressure can be found by the same operation. This technique gives flexible families of symmetric Stokes flows for solving boundary-value problems. Of course one should also symmetrize and antisymmetrize these flows with respect to inversion.

In this section I give formulas for a large enough family of such flows to solve practical problems. Some of these flows are created from others by Lie derivation with respect to rigid motions, which amounts to taking the difference of two flows with nearby ring singularities of opposite sign.

In all cases below I superpose elementary flows parametrized by an angle β located on the ring $(0, a\cos\beta, a\sin\beta)$. I take a spherical polar coordinate system (r, θ, ϕ) centered on the elementary flow with its north pole on the distinguished axis. The axis may be either in the plane of the ring ("horizontal") or perpendicular to the plane of the ring ("vertical"). The coordinates of a point $(x, y, 0)$ on C in the spherical polar coordinate system are then, in the horizontal case,

$$r = \sqrt{x^2 + y^2 + a^2 - 2ay\cos\beta} , \tag{E1}$$

$$\theta = \arccos \left[\frac{y\cos\beta - a}{r} \right] , \tag{E2}$$

$$\phi=\arcsin\left[\frac{y\sin\beta}{r\sin\theta}\right], \tag{E3}$$

and in the vertical case

$$r=\sqrt{x^2+y^2+a^2-2ay\cos\beta}, \tag{E4}$$

$$\theta=\arccos(x/r), \tag{E5}$$

$$\phi=\arcsin\left[\frac{y\sin\beta}{r\sin\theta}\right]. \tag{E6}$$

The orthonormal frame field at $(x,y,0)$ is, in the horizontal case,

$$\hat{r}=\frac{x}{r}\hat{x}+\frac{y-a\cos\beta}{r}\hat{y}-\frac{a\sin\beta}{r}\hat{z}, \tag{E7}$$

$$\hat{\theta}=\cot\theta\hat{r}-\frac{\cos\beta}{\sin\theta}\hat{y}+\frac{\sin\beta}{\cos\theta}\hat{z}, \tag{E8}$$

$$\hat{\phi}=-\frac{y\sin\beta}{r\sin\theta}\hat{x}+\frac{x\sin\beta}{r\sin\theta}\hat{y}-\frac{x\cos\beta}{r\sin\theta}\hat{z}, \tag{E9}$$

and in the vertical case

$$\hat{r}=\cos\theta\hat{x}+\frac{y-a\cos\beta}{r}\hat{y}-\frac{a\sin\beta}{r}\hat{z}, \tag{E10}$$

$$\hat{\theta}=\cot\theta\hat{r}-\csc\theta\hat{x}, \tag{E11}$$

$$\hat{\phi}=\frac{a\sin\beta}{r\sin\theta}\hat{y}+\frac{y-a\cos\beta}{r\sin\theta}\hat{z}. \tag{E12}$$

Combining with Eq. (A6) one can express the vector and tensor quantities of the Stokes flows in the local (n,s,ψ) frame if one knows them in the (r,θ,ϕ) frame. Then, integrating with respect to β, with the weight $e^{im\beta}$, gives the boundary value of a symmetric flow, just Eq. (42). For each type of elementary flow I do this for perhaps ten ring radii a, and keep the tabulated results for solving boundary-value problems. It remains to specify the basic elementary flows.

The following elementary flows are enough, and no subset seems to be enough. For each one I indicate the symmetry with respect to equatorial reflection, and whether the axis is to be regarded as horizontal or vertical, i.e., which of the above coordinate transformations is to be used. We give the flow V, the shear strain S, and the pressure P, using spherical polar coordinates and the spherical polar frame.

(i) (Even in reflection, axis horizontal):

$$V=\frac{2\cos\theta}{r^3}\hat{r}+\frac{\sin\theta}{r^3}\hat{\theta}, \tag{E13}$$

$$S=\frac{1}{r^4}\begin{bmatrix}-6\cos\theta & -3\sin\theta & 0\\ -3\sin\theta & 3\cos\theta & 0\\ 0 & 0 & 3\cos\theta\end{bmatrix}, \tag{E14}$$

$$P=0. \tag{E15}$$

(ii) (Even in reflection, axis horizontal):

$$V=\frac{\cos\theta}{r}\hat{r}-\frac{\sin\theta}{2r}\hat{\theta}, \tag{E16}$$

$$S=\frac{1}{2r^2}\begin{bmatrix}-2\cos\theta & 0 & 0\\ 0 & \cos\theta & 0\\ 0 & 0 & \cos\theta\end{bmatrix}, \tag{E17}$$

$$P=\frac{\cos\theta}{r^2}. \tag{E18}$$

(iii) (Even in reflection, axis vertical):

$$V=\frac{3(1-\cos^2)\theta}{r^4}\hat{r}-\frac{6\cos\theta\sin\theta}{r^4}\hat{\theta}, \tag{E19}$$

$$S=\frac{1}{r^5}\begin{bmatrix}-12+36\cos^2\theta & 24\sin\theta\cos\theta & 0\\ 24\sin\theta\cos\theta & 9-21\cos^2\theta & 0\\ 0 & 0 & 3-15\cos^2\theta\end{bmatrix}, \tag{E20}$$

$$P=0. \tag{E21}$$

(iv) (Even in reflection, axis vertical):

$$V=-\frac{\cos^2\theta}{r^2}\hat{r}, \tag{E22}$$

$$S=\frac{1}{r^3}\begin{bmatrix}2\cos^2\theta & \sin\theta\cos\theta & 0\\ \sin\theta\cos\theta & -\cos^2\theta & 0\\ 0 & 0 & -\cos^2\theta\end{bmatrix}, \tag{E23}$$

$$P=\frac{2(1-3\cos^2\theta)}{3r^3}. \tag{E24}$$

(v) (Odd in reflection, axis horizontal):

$$V=\frac{3\sin\theta\cos\theta\cos\phi}{r^4}\hat{r}+\frac{(\sin^2\theta-\cos^2\theta)\cos\phi}{r^4}\hat{\theta}+\frac{\cos\theta\sin\phi}{r^4}\hat{\phi}, \tag{E25}$$

$$S=\frac{1}{r^5}\begin{bmatrix}-12\sin\theta\cos\theta\cos\phi & 4(\cos^2\theta-\sin^2\theta)\cos\phi & -4\cos\theta\sin\phi\\ 4(\cos^2\theta-\sin^2\theta)\cos\phi & 7\sin\theta\cos\theta\cos\phi & -\sin\theta\sin\phi\\ -4\cos\theta\sin\phi & -\sin\theta\sin\phi & 5\sin\theta\cos\theta\cos\phi\end{bmatrix}, \tag{E26}$$

$$P=0 \ . \tag{E27}$$

(vi) (Odd in reflection, axis horizontal):

$$V=-\frac{3\sin\theta\cos\theta\cos\phi}{r^2}\hat{r}+\frac{\cos\phi}{r^2}\hat{\theta}-\frac{\cos\theta\sin\phi}{r^2}\hat{\phi} \ , \tag{E28}$$

$$S=\frac{1}{r^3}\begin{bmatrix} 6\sin\theta\cos\theta\cos\phi & -3\cos^2\theta\cos\phi & 3\cos\theta\sin\phi \\ -3\cos^2\theta\cos\phi & -3\sin\theta\cos\theta\cos\phi & 0 \\ 3\cos\theta\sin\phi & 0 & -3\sin\theta\cos\theta\cos\phi \end{bmatrix} , \tag{E29}$$

$$P=-\frac{6\cos\theta\sin\theta\cos\phi}{r^3} \ . \tag{E30}$$

(vii) (Odd in reflection, axis vertical): same elementary flow as (i).

(viii) (Odd in reflection, axis vertical): same elementary flow as (ii).

A good check of these expressions is the computation of translational and rotational drag coefficients of a rigid ellipsoid, for which analytical expressions are known. Four-place accuracy is straightforward to obtain.

For many boundary-value problems it is not good enough to represent the interior flow with ring singularities only in the equatorial plane outside the cell. One must supplement these functions with flows having singularities on rings above and below the cell, at a distance $\pm h$ from the equatorial plane. This requires replacing x by $x\pm h$ in the transformation formulas Eq. (E1)–(E12).

APPENDIX F: TANK-TREADING BOUNDARY VALUES

The shear flow

$$V=[-X\cos(\chi)+Y\sin(\chi)](\hat{x}\sin\chi+\hat{y}\cos\chi) \tag{F1}$$

evaluated on M is a linear combination of vector fields belonging to three symmetry classes: $m=0$, 1, and 2:

$$V_0=\left[-x\sin\chi\cos\chi\sin\Theta-\frac{y}{2}\sin\chi\cos\chi\cos\Theta\right]\hat{n} + \left[-x\sin\chi\cos\chi\cos\Theta+\frac{y}{2}\sin\chi\cos\chi\sin\Theta\right]\hat{s} \ , \tag{F2}$$

$$V_1=(y\sin^2\chi\sin\Theta+x\cos^2\chi)\cos\psi\hat{n} +(y\sin^2\chi\cos\Theta-x\cos^2\chi\sin\Theta)\cos\psi\hat{s} +x\cos^2\chi\sin\psi\hat{\psi} \ , \tag{F3}$$

$$V_2=-\frac{y}{2}\sin\chi\cos\chi\cos\Theta\cos2\psi\hat{n} +\frac{y}{2}\sin\chi\cos\chi\sin\Theta\cos2\psi\hat{s}-\frac{y}{2}\sin\chi\cos\chi\sin2\psi\hat{\psi} \ . \tag{F4}$$

The relevant corresponding components of the shear strain tensor are

$$S_{ns}^{(0)}=-\tfrac{3}{8}\sin2\chi\sin2\Theta \ , \tag{F5}$$

$$S_{n\psi}^{(0)}=0 \ , \tag{F6}$$

$$S_{ns}^{(1)}=\tfrac{1}{2}\cos2\chi\cos2\Theta\cos\psi \ , \tag{F7}$$

$$S_{n\psi}^{(1)}=\tfrac{1}{2}\cos2\chi\sin\Theta\sin\psi \ , \tag{F8}$$

$$S_{ns}^{(2)}=-\tfrac{1}{8}\sin2\chi\sin2\Theta\cos2\psi \ , \tag{F9}$$

$$S_{n\psi}^{(2)}=\tfrac{1}{4}\sin2\chi\cos\Theta\sin2\psi \ . \tag{F10}$$

Since we are matching to complex solutions transforming under rotation by multiplication by $e^{im\psi}$, we should also regard the above components in this way, i.e.,

$$V_m(s,\psi)=\mathrm{Re}[V_m'(s)e^{im\psi}] \ , \tag{F11}$$

$$S^{(m)}(s,\psi)=\mathrm{Re}[S_m'(s)e^{im\psi}] \ , \tag{F12}$$

where V_m' and S_m' are complex. Then we can just match the s-dependent functions on C, replacing $\cos m\psi$ by 1 and $\sin m\psi$ by $-i$ in Eqs. (F2)–(F10). One has to solve the following inhomogeneous linear system of equations in each symmetry class for flows V^{out}, V^{in}, and V^M,

$$V'=-V^{\mathrm{out}}+V^M \ , \tag{F13}$$

$$0=-V^{\mathrm{in}}+V^M \ , \tag{F14}$$

$$2\eta_{\mathrm{out}}S_{nj}'=-2\eta_{\mathrm{out}}S_{nj}^{\mathrm{out}}+2\eta_{\mathrm{in}}S_{nj}^{\mathrm{in}} +2\eta_M\mathrm{div}(S_M)_j+\Pi_{,j} \ , \tag{F15}$$

matching velocities and tangential stresses on M. The gradient of an arbitrary two-dimensional pressure Π in the preceding equation comes from incompressibility of the membrane.

The net torque applied by the external fluid to M about the z axis belongs to the $m=1$ symmetry class. Writing simply S for $S'+S^{\mathrm{out}}$ on C, it is

$$\tau=2\pi\eta_{\mathrm{out}}\int_0^{\pi/2}[2\,\mathrm{Re}S_{ns}(x\sin\Theta-y\cos\Theta)+2\,\mathrm{Im}S_{n\psi}x +\mathrm{Re}P(x\cos\Theta+y\sin\Theta)]y\,ds \ . \tag{F16}$$

When I have found the value of χ for which τ is zero, I solve the linear system in the $m=0$ and 2 symmetry classes as well, and from the solutions I find the normal stress $P^{\mathrm{in}}-P^{\mathrm{out}}$ which deforms the cell.

[1] E. Evans and R. Skalak, *Mechanics and Thermodynamics of Biomembranes* (CRC, Boca Raton, FL, 1980).
[2] R. M. Hochmuth, in *Properties of Red Blood Cells, Handbook of Bioengineering,* edited by R. Skalak and S. Chien (McGraw-Hill, New York, 1987).
[3] B. T. Stokke, A. Mikkelsen, and A. Elgsaeter, Biophys. J. **49**, 319 (1986).
[4] L. Radzihovsky and D. R. Nelson, Phys. Rev. A **44**, 3525 (1991).
[5] R. Lipowsky and M. Girardet, Phys. Rev. Lett. **65**, 2893 (1990).
[6] W. Helfrich, J. Phys. (Paris) **46**, 1263 (1985).
[7] E. Evans and W. Rawicz, Phys. Rev. Lett. **64**, 2094 (1990).
[8] S. J. Singer and G. L. Nicolson, Science **175**, 720 (1972).
[9] E. Evans and R. M. Hochmuth, J. Membr. Biol. **30**, 351 (1977).
[10] F. Brochard and J. F. Lennon, J. Phys. (Paris) **36**, 1035 (1975).
[11] K. Zeman, H. Engelhardt, and E. Sackmann, Eur. Biophys. J. **18**, 203 (1990).
[12] H. Engelhardt, H. Gaub, and E. Sackmann, Nature **307**, 378 (1984).
[13] M. Bessis and N. Mohandas, Blood Cells **1**, 307 (1975).
[14] T. Fischer and H. Schmid-Schoenbein, Blood Cells **3**, 351 (1977).
[15] T. J. Willmore, *An Introduction to Differential Geometry* (Clarendon, Oxford, 1966).
[16] B. Schutz, *Geometrical Methods to Mathematical Physics* (Cambridge University Press, Cambridge, 1980).
[17] S. Svetina and B. Zeks, Eur. Biophys. J. **17**, 101 (1989).
[18] H. J. Deuling and W. Helfrich, Biophys. J. **16**, 861 (1976).
[19] J. T. Jenkins, J. Math. Biol. **4**, 149 (1977).
[20] W. Helfrich, Z. Naturforsch. **C28**, 693 (1973). In this seminal paper Helfrich writes the integrand of E_B as $(2H-c_0)^2$. I have rewritten it to emphasize the probable role of c_0 as a Lagrange multiplier.
[21] K. Berndl, J. Kaes, R. Lipowsky, E. Sackmann, and U. Seifert, Europhys. Lett. **13**, 659 (1990).
[22] M. Peterson, E. Sackmann, and H. Strey (unpublished).
[23] R. M. Servuss, W. Harbich, and W. Helfrich, Biochem. Biophys. Acta **436**, 900 (1976).
[24] M. B. Schneider, J. T. Jenkins, and W. W. Webb, J. Phys. (Paris) **45**, 1457 (1984).
[25] H. P. Duwe, J. Kaes, and E. Sackmann, J. Phys. (Paris) **51**, 945 (1990).
[26] R. Grebe, Diploma thesis, Rheinland-Westfalen Technische Hochschule, Aachen, 1990 (unpublished).
[27] H. S. Kage, J. Raedler, and H. Strey (private communication).
[28] H. S. Kage, Diploma thesis, Technische Universität Muenchen, 1988 (unpublished).
[29] M. A. Peterson, J. Math. Phys. **26**, 711 (1985).
[30] S. R. Keller and R J. Skalak, J. Fluid Mech. **120**, 22 (1982).
[31] T. M. Fischer, M. Stoehr-Liesen, and H. Schmid-Schoenbein, Science **202**, 894 (1978).
[32] T. M. Fischer, M. Stoehr, and H. Schmid-Schoenbein, AlChE Symp. Ser. **182**, 38 (1978).
[33] M. A. Peterson, Mol. Cryst.-Liq. Cryst. **127**, 257 (1985). There is a factor of 2 error in this paper. The internal and external viscosities η_i and η_e should be replaced by $2\eta_i$ and $2\eta_e$.
[34] F. E. Weaver, H. Polster, P. Febboriello, M. P. Sheetz, H. Schmid-Schoenbein, and D. E. Koppel, Biophys. J. **58**, 1427 (1990).
[35] M. A. Peterson, J. Appl. Phys. **57**, 1739 (1985).